ARTICLE IN PRESS – Acta Cryst. B

STRUCTURAL SCIENCE
CRYSTAL ENGINEERING
MATERIALS

ISSN 2052-5206

$Rb_2CaCu_6(PO_4)_4O_2$, a novel oxophosphate with a shchurovskyite-type topology: synthesis, structure, magnetic properties and crystal chemistry of rubidium copper phosphates$Rb_2CaCu_6(PO_4)_4O_2$

Proof instructions

Proof corrections should be returned by **23 July 2019**. After this period, the Editors reserve the right to publish your article with only the Managing Editor's corrections.

Please
(1) Read these proofs and assess whether any corrections are necessary.
(2) Check that any technical editing queries highlighted in **bold underlined** text have been answered.
(3) Send corrections by e-mail to **actab@iucr.org**. Please describe corrections using plain text, where possible, giving the line numbers indicated in the proof. Please do not make corrections to the pdf file electronically and please do not return the pdf file. If no corrections are required please let us know.

To arrange payment for **open access**, please visit **http://scripts.iucr.org/openaccess/?code=ra5054**. To purchase printed offprints, please complete the attached order form and return it by e-mail.

Please check the following details for your article

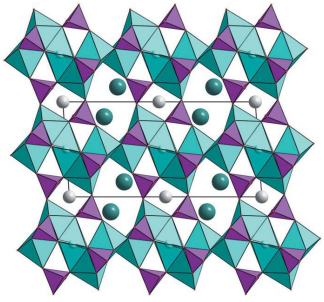

Thumbnail image for contents page

Synopsis: A novel compound, $Rb_2CaCu_6(PO_4)_4O_2$, was synthesized by a hydrothermal method and characterized as the shchurovskyite-type structure, based upon a heteropolyhedral copper phosphate framework. Microscopic calculations are indicative of possible low-dimensional magnetic behavior, as they confirm weak magnetic coupling between the copper-based layers mediated by the Cu–Cu pairs.

Abbreviated author list: Aksenov, S.M.; Borovikova, E.Y. (0000-0002-9003-3695); Mironov, V.S. (0000-0001-7313-8279); Yamnova, N.A.; Volkov, A.S.; Ksenofontov, D.A.; Gurbanova, O.A.; Dimitrova, O.V.; Deyneko, D.V. (0000-0002-9422-1925); Zvereva, E.A.; Maximova, O.V.; Krivovichev, S.V. (0000-0001-8352-1394); Burns, P.C.Vasiliev, A.N.

Keywords: hydrothermal synthesis; copper oxophosphate; shchurovskyite; single-crystal X-ray diffraction; IR spectroscopy; structural complexity; magnetic properties

How to cite your article in press

Your article has not yet been assigned page numbers, but may be cited using the doi:

Aksenov, S.M., Borovikova, E.Y., Mironov, V.S., Yamnova, N.A., Volkov, A.S., Ksenofontov, D.A., Gurbanova, O.A., Dimitrova, O.V., Deyneko, D.V., Zvereva, E.A. *et al*. (2019). *Acta Cryst.* B**75**, https://doi.org/10.1107/S2052520619008527.

Acta Cryst B
STRUCTURAL SCIENCE
CRYSTAL ENGINEERING
MATERIALS
ISSN 2052-5206

$Rb_2CaCu_6(PO_4)_4O_2$, a novel oxophosphate with a shchurovskyite-type topology: synthesis, structure, magnetic properties and crystal chemistry of rubidium copper phosphates

Sergey M. Aksenov,[a,b]* Elena Yu. Borovikova,[c] Vladimir S. Mironov,[b] Natalia A. Yamnova,[c] Anatoly S. Volkov,[c] Dmitry A. Ksenofontov,[c] Olga A. Gurbanova,[c] Olga V. Dimitrova,[c] Dina V. Deyneko,[c] Elena A. Zvereva,[c] Olga V. Maximova,[c,d] Sergey V. Krivovichev,[e,f] Peter C. Burns[a,g] and Alexander N. Vasiliev[c,d,e]

[a]Department of Civil and Environmental Engineering and Earth Sciences, University of Notre Dame, Notre Dame, Indiana 46556, USA, [b]Institute of Crystallography of FSRC 'Crystallography and Photonics', RAS, Leninskii pr. 59, Moscow, 119333, Russian Federation, [c]Moscow State University, Vorobievy Gory, Moscow, 119991, Russian Federation, [d]National University of Science and Technology 'MISiS', Leninskii pr. 4, Moscow, 119049, Russian Federation, [e]St Petersburg State University, University Embankment 7/9, St Petersburg, 199034, Russian Federation, [f]Kola Science Centre, Russian Academy of Sciences, Fersmana 14, Apatity, Murmansk region 184209, Russian Federation, and [g]Department of Chemistry and Biochemistry, University of Notre Dame, Notre Dame, IN 46556, USA. *Correspondence e-mail: aks.crys@gmail.com

Received 13 February 2019
Accepted 14 June 2019

Edited by R. Černý, University of Geneva, Switzerland

Keywords: hydrothermal synthesis; copper oxophosphate; shchurovskyite; single-crystal X-ray diffraction; IR spectroscopy; structural complexity; magnetic properties.

CCDC reference: 1870440

Supporting information: this article has supporting information at journals.iucr.org/b

Single crystals of $Rb_2CaCu_6(PO_4)_4O_2$ were synthesized by a hydrothermal method in the multicomponent system $CuCl_2$–$Ca(OH)_2$–RbCl–B_2O_3–Rb_3PO_4. The synthesis was carried out in the temperature range from 690 to 700 K and at the general pressure of 480–500 atm [**1 atm = 101.325 kPa**] from the mixture in the molar ratio 2CuO:CaO:Rb_2O:B_2O_3:P_2O_5. The crystals studied by single-crystal X-ray analysis were found to be monoclinic, space group $C2$, a = 16.8913 (4), b = 5.6406 (1), c = 8.3591 (3) Å, β = 93.919 (3)°, V = 794.57 (4) Å^3. The crystal structure of $Rb_2CaCu_6(PO_4)_4O_2$ is similar to that of shchurovskyite and dmisokolovite and is based upon a heteropolyhedral open framework formed by polar layers of copper polyhedra linked *via* isolated PO_4 tetrahedra. The presence of well-isolated 2D heteropolyhedral layers in the title compound suggests low-dimensional magnetic behavior which is masked however by the fierce **competition between** multiple ferromagnetic and antiferromagnetic exchange interactions. At T_C = 25 K, $Rb_2CaCu_6(PO_4)_4O_2$ reaches a magnetically ordered state with large residual magnetization.

1. Introduction

Alkaline phosphates with transition metals attract interest because of their broad technological applications as battery materials, sorbents, catalysts, ion-exchangers *etc.* (Cheetham *et al.*, 1999; Maspoch *et al.*, 2007; Williams *et al.*, 2013; Whittingham, 2014; Yakubovich *et al.*, 2016). Among these, copper pyrophosphates are of interest because of their magnetic structures of different dimensionalities (Shvanskaya *et al.*, 2013; Mannasova *et al.*, 2016).

Typically, the coordination environment of the Cu^{2+} cation in oxygen compounds is a distorted octahedron (due to the Jahn–Teller effect) (Burns & Hawthorne, 1995*a*,*b*; Krivovichev, Filatov & Vergasova, 2013). However, the coordination number may be reduced to five or four, due to some local crystal-chemical requirements. For instance, the recently described crystal structure of $(Rb,K)_2Cu_3(P_2O_7)_2$ is characterized by the simultaneous presence of CuO_6 octahedra

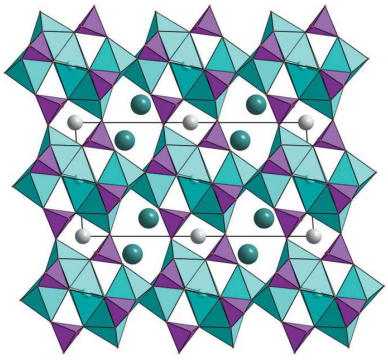

and CuO_5 pyramids (Krivovichev & Chernyat'eva, 2016). Among minerals, natural copper arsenates shchurovskyite, $K_2CaCu_6(AsO_4)O_2$, and dmisokolovite, $K_3Cu_5Al(AsO_4)O_2$, found in sublimates of the Arsenatnaya fumarole (Tolbachik volcano, Kamchatka, Russia), have three types of Cu^{2+} coordination environments: CuO_6 octahedra, CuO_5 pyramids and CuO_4 squares (Pekov *et al.*, 2015, 2018). In the structures of copper oxysalts CuO_n polyhedra can build cationic motifs of different dimensionalities (from isolated polyhedra to heteropolyhedral frameworks). A classification of minerals and inorganic compounds has been proposed based on the polymerization of CuO_4 squares (Leonyuk *et al.*, 1998, 2001).

Oxysalts with mineral-like structures containing 'additional' oxygen atoms and OH groups that can be described in terms of anion-centered tetrahedra (Krivovichev & Filatov, 2001; Krivovichev, Mentré *et al.*, 2013) as having anion-centered [$(OH)Me_3$] triangles and [OMe_4] tetrahedra (Me = Cu, Ni, Fe, Zn *etc*.) attract interest due to their magnetic properties controlled by the local structure of the oxygen-based copper polycations (Aksenov *et al.*, 2017; Yamnova *et al.*, 2017; Volkova & Marinin, 2017, 2018*a*,*b*).

In this paper we report on the hydrothermal synthesis, single-crystal X-ray structure analysis and IR spectra of a novel oxy [**or oxo?**]phosphate $Rb_2CaCu_6(PO_4)_4O_2$; we evaluate the magnitude and sign-of-spin coupling between magnetic Cu^{2+} ions and discuss the possible manifestation of low-dimensional magnetic behavior of this compound. The crystal-chemical features and structural complexity of rubidium copper phosphates and related oxysalts are also discussed.

2. Experimental

2.1. Synthesis and sample characterization

Single crystals of $Rb_2CaCu_6(PO_4)_4O_2$ were synthesized by a hydrothermal method in the multicomponent system $CuCl_2$–$Ca(OH)_2$–RbCl–B_2O_3–Rb_3PO_4. The synthesis was carried out in the temperature range from 690 to 700 K and at the general pressure of 480–500 atm [**1 atm = 101.325 kPa**] from the oxide mixture in the molar ratio $2CuO:CaO:Rb_2O:B_2O_3:P_2O_5$. A standard Cu-lined stainless steel autoclave of 16 ml capacity was used. The coefficient of the autoclave filling was selected so that the pressure was constant. The **heating time** was 20 days and corresponds to the full completion of the chemical reaction. **The product was then cooled to room temperature over 24 h.** The precipitate was separated by filtration, washed several times with hot distilled water and finally dried at room temperature for 12 h. The reaction products were small green crystals of the new phase $Rb_2CaCu_6(PO_4)_4O_2$ (Fig. 1) in 15% yield, light blue crystals of $CaCu_2(PO_4)_2$ and deep blue crystals of CuB_2O_4. The crystals of $Rb_2CaCu_6(PO_4)_4O_2$ were selected manually for further studies.

(*a*) (*b*)

Figure 1
A photograph of crystals of the $Rb_2CaCu_6(PO_4)_4O_2$ compound (*a*) and a scanning electron microscopy image showing the crystal morphology (*b*).

The elemental contents (Fig. S1, Table S1, in the supporting information) of the selected crystals were determined by a Jeol JSM6480LV scanning electron microscope equipped with an INCA Wave 500 wavelength spectrometer. The conditions of analysis were: accelerating voltage 20 kV, current 20 nA, beam diameter 3 μm.

2.2. Vibrational spectroscopy

The IR spectrum of $Rb_2CaCu_6(PO_4)_4O_2$ was obtained using an FSM 12011 FTIR spectrometer using the KBr disc technique in the wavenumber region from 4000 to 400 cm^{-1}. The spectral resolution was about 2 cm^{-1}.

The IR absorption spectrum is shown in Fig. 2. The bands in the region 1100–400 cm^{-1} are due to phosphate units. Theoretical group analysis for the tetrahedral phosphate ion PO_4^{3-} in a local position with C_1 symmetry and C_2 factor group leads to the following allowed IR vibrations: $\nu_3 - 3A + 3B$, $\nu_1 - A + B$, $\nu_4 - 3A + 3B$ and $\nu_2 - 2A + 2B$ for each of the two independent phosphorus sites. IR bands observed at 1109, 1060, 1036, 1015, 1002, 963 cm^{-1} are assigned to the antisymmetric stretching ν_3 modes of PO_4^{3-} units. The IR bands at 950 and 925 cm^{-1} are attributed to the phosphate ions ν_1 symmetric stretching modes. The IR bands in the region 640–470 cm^{-1} are due to antisymmetric bending ν_4 vibrations. The bands at 452 and 418 cm^{-1} are assigned to ν_2 symmetric bending vibrations. Because of the proximity and partial overlapping of many vibrations, the observed number of

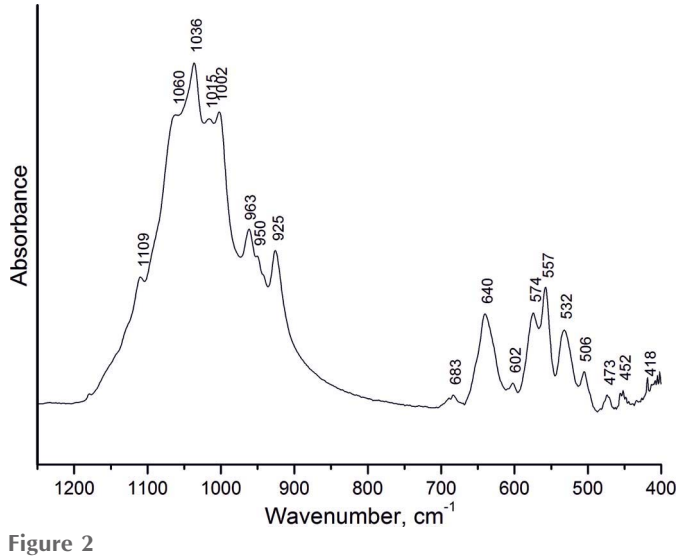

Figure 2
IR spectrum of $Rb_2CaCu_6(PO_4)_4O_2$ at room temperature.

Table 1
Experimental details **Generated from cif**.

Crystal data	
Chemical formula	$CaCu_6O_{18}P_4Rb_2$
M_r	1004.2
Crystal system, space group	Monoclinic, *C*2
Temperature (K)	293
a, *b*, *c* (Å)	16.8913 (4), 5.6406 (1), 8.3591 (3)
β (°)	93.919 (3)
V (Å^3)	794.57 (4)
Z	2
Radiation type	Mo *K*α
Wavelength (Å)	**0.71069**
μ (mm^{-1})	14.80
Crystal size (mm)	0.24 × 0.22 × 0.15
Data collection	
Diffractometer	Xcalibur, Sapphire3 with high theta cut**-off**
Absorption correction	Multi-scan
T_{min}, T_{max}	0.488, 1.000
No. of measured, independent and observed [$I > 2\sigma(I)$] reflections	21970, 5108, 3914
R_{int}	0.064
(sin $\theta/\lambda)_{max}$ (Å^{-1})	1.168
Refinement	
$R[F^2 > 2\sigma(F^2)]$, $wR(F^2)$, *S*	0.050, 0.050, 0.97
No. of reflections	5108
No. of parameters	153
$\Delta\rho_{max}$, $\Delta\rho_{min}$ (e Å^{-3})	1.21, −1.26
Absolute structure	**0 of Friedel pairs used in the refinement [Section editor comment: No absolute structure parameter??**

signals in all regions of the IR spectrum is lower than is allowed by the selection rules.

2.3. X-ray powder diffraction and single-crystal analysis

Powder X-ray diffraction data of $Rb_2CaCu_6(PO_4)_4O_2$ (Fig. S2) were collected with a Stoe-Stadi MP (Stoe & Cie Gmbh, Darmstadt, Germany) powder diffractometer equipped with a curved Ge(111) monochromator to provide strictly monochromatic Co $K\alpha_1$ radiation, 40 kV, 35 mA. The data were acquired by successively covering the scanning region using a position-sensitive linear detector with 2θ **or** $\Delta(2\theta)$ = 5° and a channel width of 0.02°.

A green unshaped grain of $Rb_2CaCu_6(PO_4)_4O_2$ (0.13 × 0.15 × 0.18 mm) was selected carefully under a polarizing microscope and used for single-crystal X-ray data collection. The single-crystal X-ray data were collected at room temperature on an Oxford Diffraction Xcalibur S diffractometer with graphite monochromated Mo *K*α radiation (λ = **0.71073** Å) and a CCD detector using the ω scanning mode. Raw data were integrated and then scaled, merged and corrected for Lorentz–polarization effects using the *CrysAlis* package (Oxford Diffraction, 2009). The following unit-cell parameters have been obtained by the least-squares refinement: *a* = 16.8913 (4), *b* = 5.6406 (1), *c* = 8.3591 (3) Å, β = 93.919 (3)°, *V* = 794.57 (4) Å^3. Space group *C*2 (No. 5) was chosen based on the reflection statistics and was confirmed by the successful

Table 2
Selected interatomic distances (Å) for $Rb_2Ca\{Cu_6O_2(PO_4)_4\}$ **Should symmetry operations be given?**.

Bond	Distance	Bond	Distance
Rb—O9	2.814 (3)	Ca—O6	2.312 (3) ×2
Rb—O1	**2.876 (3)**	Ca—O5	2.423 (3) ×2
Rb—O6	**2.940 (3)**	Ca—O3	2.575 (3) ×2
Rb—O7	3.074 (3)	Ca—O7	2.970 (4) ×2
Rb—O1	3.133 (3)	Mean	**2.570 (X)**
Rb—O7	3.278 (4)	Cu4—O7	1.899 (4)
Rb—O8	3.424 (3)	Cu4—O4	**1.907 (3)**
Mean	**3.077 (X)**	Cu4—O3	2.104 (3)
Cu1—O4	1.902 (2)	Cu4—O5	2.146 (3)
Cu1—O1	1.937 (3)	Cu4—O9	2.253 (2)
Cu1—O8	1.959 (3)	Mean	**2.062 (X)**
Cu1—O9	2.075 (3)	**Cu—O6**†	2.729 (3)
Cu1—O8	2.407 (3)	P1—O9	**1.536 (2)**
Mean	**2.056 (X)**	P1—O3	1.540 (3)
Cu2—O4	1.913 (2) ×2	P1—O8	**1.544 (3)**
Cu2—O2	1.922 (3) ×2	P1—O2	1.568 (3)
Mean	**1.918 (X)**	Mean	**1.548 (X)**
Cu2—O6†	2.968 (3) ×2	P2—O6	1.517 (3)
Cu3—O4	**1.925 (2)** ×2	P2—O2	1.536 (3)
Cu3—O2	1.993 (3) ×2	P2—O7	**1.553 (3)**
Cu3—O5	2.473 (3) ×2	P2—O5	1.557 (3)
Mean	**2.131 (X)**	Mean	1.541

† Not considered in the calculation of the average bond length, but has been included in the calculation of the bond-valence sums.

Table 3
Bond-valence calculation for $Rb_2Ca\{Cu_6O_2(PO_4)_4\}$.

$\sum_v$a and $\sum_v$c are the bond-valence sums for anions and cations, respectively. The ×2↓ sign indicates the doubling of the corresponding valence contributions in columns due to symmetry.

Site	Rb	Cu1	Cu2	Cu3	Cu4	Ca	P1	P2	$\sum_v$a
O1	0.19+0.10	0.49						1.24	2.02
O2			$0.51_{\times2\downarrow}$	$0.42_{\times2\downarrow}$			1.14		2.07
O3					0.31	$0.19_{\times2\downarrow}$	1.23		1.73
O4		0.54	$0.52_{\times2\downarrow}$	$0.50_{\times2\downarrow}$	0.53				2.09
O5				$0.11_{\times2\downarrow}$	0.27	$0.29_{\times2\downarrow}$		1.18	1.85
O6	0.16		$0.03_{\times2\downarrow}$		0.05	$0.39_{\times2\downarrow}$		1.31	1.94
O7	0.11+0.06				0.54	$0.07_{\times2\downarrow}$		1.19	1.97
O8	0.04	0.46+0.13					1.21		1.84
O9	0.23	0.33			0.20		1.24		2.00
$\sum_v$c	0.89	1.95	2.12	2.06	1.90	1.88	4.82	4.92	

refinement of the structure. The experimental details of the data collection and refinement results are listed in Table 1.

A structure model was produced by the 'charge flipping' method using the *SUPERFLIP* computer program (Palatinus & Chapuis, 2007). The structure determinations and refinements were carried out using the *Jana2006* program package (Petříček *et al.*, 2006). Atomic scattering factors for neutral atoms together with anomalous dispersion corrections were taken from *International Tables for Crystallography* (Prince, 2006). Illustrations were produced with the *Jana2006* program package in combination with the program *DIAMOND* (Brandenburg & Putz, 2005). Table S2 lists the fractional atomic coordinates, occupancy, site symmetries and equivalent atomic displacement parameters (U_{eq}). Anisotropic atomic displacement parameters (U_{ij}) are presented in Table S3. Selected interatomic distances are given in Table 2.

Bond-valence sums (BVS, Table 3) were calculated using the bond-valence parameters for Cu^{2+}—O bonds (Krivo-

vichev, 2012*a*) and for other bonds (Rb^{+}—O, Ca^{2+}—O and P^{5+}—O) (Brown & Altermatt, 1985).

2.4. Theoretical study of magnetic properties

To examine the low-dimensional properties of $Rb_2CaCu_6(PO_4)_4O_2$, we evaluated the magnitude and sign-of-spin coupling $J\mathbf{S}_i\mathbf{S}_j$ between Cu^{2+} ions within the 2D networks and between them (Fig. 3). For each Cu···Cu exchange-coupled pair, the exchange parameters J were obtained from numerical calculations in terms of a microscopic many-electron superexchange model using a computational scheme (Mironov *et al.*, 2003; Nikiforova *et al.*, 2011; Zorina *et al.*, 2013). In these calculations, the electronic structure and magnetic characteristics of the individual Cu^{2+} ions located in the different copper sites are treated in terms of ligand-field (LF) calculations combined with the angular-overlap model (AOM) (Schaffer, 1968); the latter provides more consistent information on the orbital composition of the ground-state wavefunctions of Cu^{2+} ions in the low-symmetry coordination polyhedra CuO_n [Fig. 4(*a*)]. The AOM parameters used for Cu^{2+} ions are e_σ = 4000 and e_π = 1000 cm^{-1} (at the reference metal–ligand distance R_0 = 2.15 Å); the radial dependence of these parameters is approximated by $e_{\sigma,\pi}(R) = e_{\sigma,\pi}(R_0)\,(R_0/R)^n$ with n = 4. Furthermore, we used B = 900 and C = 4000 cm^{-1} Racah parameters (for the $3d^9$ charge-transfer state of copper ions) and ζ = 650 cm^{-1} spin–orbit coupling constant. Exchange parameters J were calculated for all actual Cu–Cu exchange-coupled pairs in the crystal structure of $Rb_2CaCu_6(PO_4)_4O_2$, in which adjacent Cu^{2+}(1–4) ions are bridged by oxygen atoms and/or tetrahedral PO_4 phosphate groups [Figs. 4(*b*) and 4(*c*)]. It is noteworthy that the key elements of the superexchange theory are electron transfer parameters t_{ij}, which are one-electron matrix elements connecting magnetic 3*d* orbitals on two exchange-coupled transition-metal centers A and B, $t_{ij} = \langle 3d_i(A)|h|3d_j(B)\rangle$; in fact, exchange parameters J are very sensitive to the set of electron transfer parameters t_{ij}. In our calculations, these matrix elements are obtained from molecular orbital (MO) calculations in terms of the extended Hückel theory (EHT) using atomic EHT parameterization available from http://www.op.titech.ac.jp/lab/mori/EHTB/EHTB.htm [**URL not found, please check**]. More specifically, the EHT calculations were performed for clusters involving two adjacent copper atoms and their extended atomic surroundings involving bridging and terminal oxygen atoms and tetrahedral PO_4 groups; examples are shown in Fig. 3. The local structure of these clusters corresponds to the actual crystal structure of $Rb_2CaCu_6(PO_4)_4O_2$. The electron transfer parameters t_{ij} are derived by projection of the ten most 3*d*-rich molecular orbitals of the Cu(A)···Cu(B) pair onto purely atomic 3*d* orbitals of two copper atoms A and B (Lee, 1989; Nikiforova *et al.*, 2011; Zorina *et al.*, 2013). The Cu(A)↔Cu(B) charge-transfer energy is set to 65000 cm^{-1} (8 eV); this approach has been previously applied to analyze the spin-coupling mechanism in 3*d*-based molecular magnets (Nikiforova *et al.*, 2011).

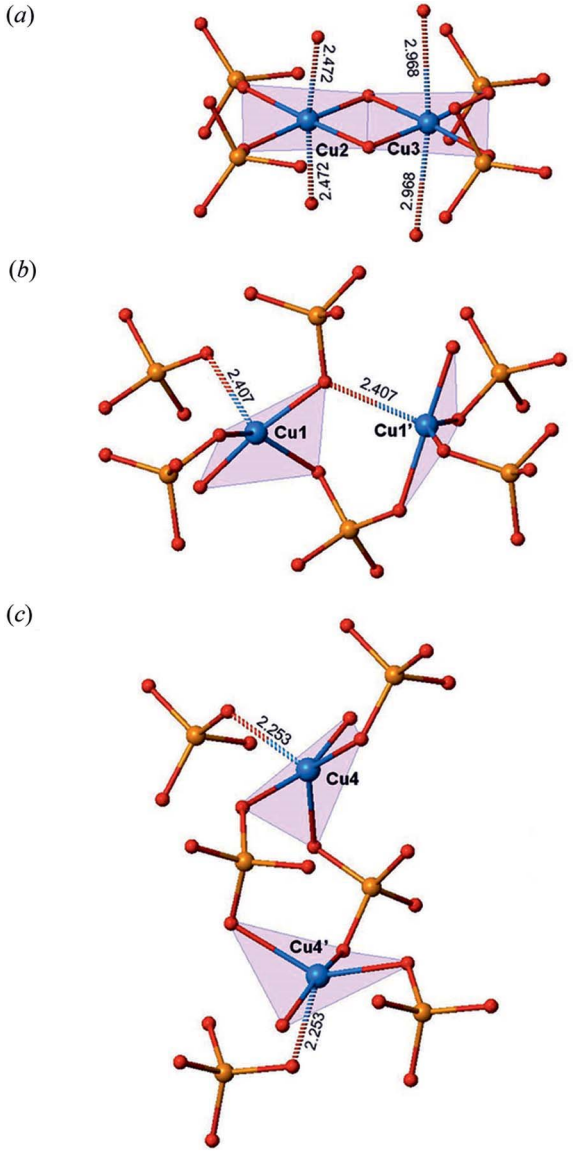

Figure 3
Examples of the local structure of exchange-coupled pairs Cu–Cu in $Rb_2CaCu_6(PO_4)_4O_2$ employed for microscopic superexchange calculations. The basic CuO_4 squares of copper sites are **marked[shaded]** in pink[lilac/light purple?]. Distances are given in Å**Are these coordination polyhedra? Why are s.u.'s missing on distances? These numbers are too small and should be given in caption.**

2.5. Structural complexity calculation

The structural complexity of the crystal structures was measured using Shannon information per atom (I_G) and per reduced unit cell ($I_{G,total}$):

$$I_G = -\sum_{i=1}^{k} p_i \log_2 p_i \text{ (bits per atom)} \quad (1)$$

$$I_{G,total} = -vI_G = -v\sum_{i=1}^{k} p_i \log_2 p_i \text{ (bits per unit cell)} \quad (2)$$

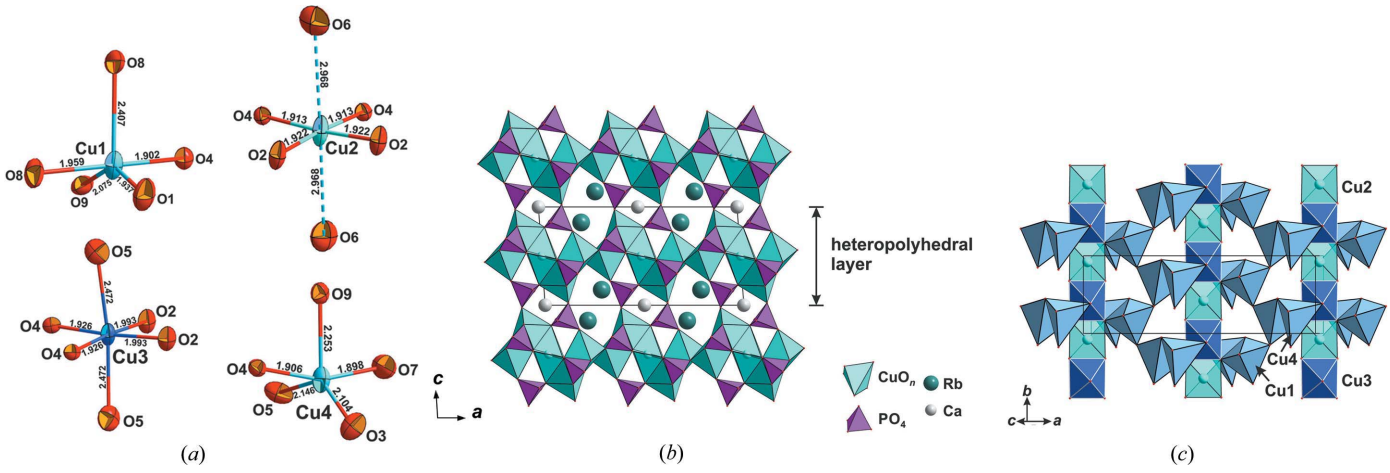

Figure 4
General view of the crystal structure of $Rb_2CaCu_6(PO_4)_4O_2$ **(distances in Å)** (*a*), heteropolyhedral layer (*b*) and coordination environment of copper polyhedra (*c*). **Why are s.u.'s missing on distances? These numbers are too small and should be given in caption. [or refer to Table 2 if appropriate**

Table 4
Calculated anisotropic *g*-tensor of copper sites [Fig. 2(*b*)].

	g-tensor components		
Copper site	g_1	g_2	g_3
Cu1	2.025	2.127	2.363
Cu2	2.058	2.058	2.317
Cu3	2.064	2.067	2.348
Cu4	1.997	2.219	2.331

where k is the number of different crystallographic orbits and p_i is the random-choice probability for an atom from the ith crystallographic orbit, that is

$$p_i = m_i/v \qquad (3)$$

where m_i is the multiplicity of a crystallographic orbit relative to the reduced unit cell, and v is the number of atoms in the reduced unit cell (= number of vertices in the quotient graph) (Krivovichev, 2012*b*, 2013*a*). This approach was successfully used to characterize the complexity of minerals, zeolites and different types of inorganic compounds (Krivovichev, 2013*b*; Siidra *et al.*, 2014; Grew *et al.*, 2016; Hazen *et al.*, 2017). Complexity parameters for the whole structure have been calculated using the software *TOPOS* (Blatov *et al.*, 2014).

3. Results

3.1. Crystal structure

The crystal structure of $Rb_2CaCu_6(PO_4)_4O_2$ is similar to those of shchurovskyite, $K_2CaCu_6(AsO_4)_4O_2$, and dmisokolovite, $K_3Cu_5(AsO_4)_4O_2$ (Table 4), and is based upon a heteropolyhedral open framework formed by polar Cu-based oxo layers linked *via* isolated PO_4 tetrahedra (Fig. 5).

The layer is formed by CuO_n polyhedra of three types: square ($n = 4$), square-pyramid ($n = 5$) and octahedron ($n = 6$). It is based upon rods of edge-sharing $Cu2O_4$ squares and $Cu3O_6$ octahedra [the Cu2···Cu3 distance is 2.775 (1) Å] extending along [010]. The $Cu2O_4$ square has two long (2.968 Å) distances to the O6 atoms [comparable with that observed in the structure of shchurovskyite (Pekov *et al.*, 2015)], so the coordination environment of the Cu2 site can be considered as a Jahn–Teller-distorted (4+2)-tetragonal bipyramid [which is common for inorganic oxysalts (Burns & Hawthorne, 1995*a*,*b*; **Krivovichev *et al.*, 2013 [two Krivovichev et al. 2013 references, please indicate which]**)]. However, the bond-valence contribution of this bond is low [0.03 valence units (v.u.); Table 3], which allows us to treat the $Cu2O_n$

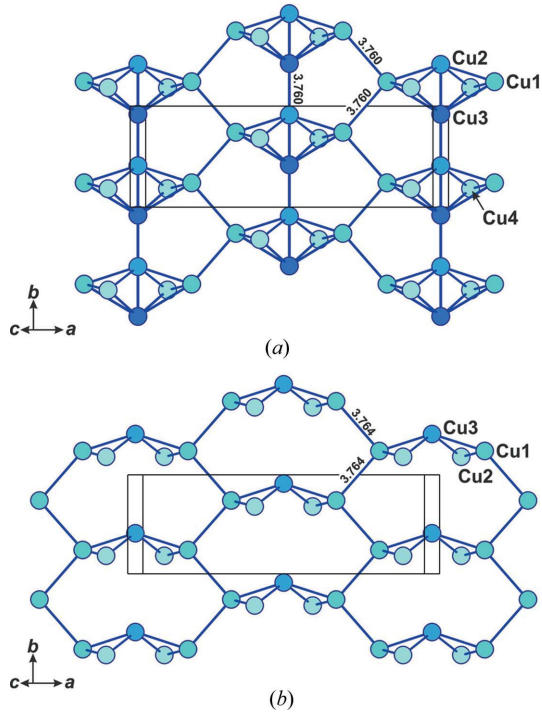

Figure 5
Copper net in the crystal structures of $Rb_2CaCu_6(PO_4)_4O_2$ and shchurovskyite (*a*) and **dmisokolovite** (*b*). **Distances in Å. Why are s.u.'s missing on distances? These numbers are too small and should be given in caption.**

polyhedron as a planar square. Each rod is decorated by 'additional' $Cu1O_5$ and $Cu4O_5$ distorted square-pyramids [Fig. 5(*a*)]. Apical vertices of these pyramids are parallel to each other and elongated along [010], resulting in the non-centrosymmetric (polar) character of the layers. Adjacent rods are linked by sharing common vertices of the $Cu1O_5$ polyhedra.

In the crystal structures of $Rb_2CaCu_6(PO_4)_4O_2$ and shchurovskyite, Cu atoms form rather complex cationic 2D arrays (Pekov *et al.*, 2015). Replacement of one Cu atom by Al in the crystal structure of dmisokolovite (Pekov *et al.*, 2015) leads to another type of low-dimensional topology of Cu atoms [Fig. 5(*b*)].

Heteropolyhedral Cu-based layers are linked *via* isolated PO_4 tetrahedra forming a 3D framework with the composition $\{Cu_6O_2(PO_4)_4\}^{3-}$, containing wide channels occupied by both alkaline (Rb^+) and alkaline-earth (Ca^{2+}) cations. The density of the framework (FD) is 25.17 Cu+P atoms per 1 nm^3. Despite the fact that the ionic radius of rubidium (rRb^{VII} = 1.56 Å) is considerably larger than that of potassium (rK^{VII} = 1.46 Å), the unit-cell volume of shchurovskyite-type compounds predominantly depends on the ionic radii of the tetrahedrally coordinated cations. Therefore, the unit-cell volume of $Rb_2CaCu_6(PO_4)_4O_2$ (V = 794.57 $Å^3$) is smaller than that of shchurovskyite $K_2CaCu_6(AsO_4)_4O_2$ (V = 839.24 $Å^3$).

The crystal structure of $Rb_2CaCu_6(PO_4)_4O_2$ contains two types of parallel channels extending along [010]. Channel I is delimited by four CuO_n polyhedra and four PO_4 tetrahedra and has a distorted hexagonal cross section. The effective width (e.c.w.) of channel I, calculated (McCusker *et al.*, 2003) by subtracting the ionic diameter of O^{2-} (2.7 Å) from the shortest and longest O···O distances across the channel, is 2.6 × 5.7 Å (the O7–O7 and O8–O8 distances, respectively). Channel I is filled by Rb atoms (Fig. S3*a*). Channel II is delimited by two CuO_n polyhedra and two PO_4 tetrahedra and has a tetragonal cross section (e.c.w. = 0.9 × 1.3 Å, measured using the O5···O5 and O7···O7 distances). This channel is filled by Ca^{2+} cations (Fig. S3*b*).

The crystal structures of $Rb_2CaCu_6(PO_4)_4O_2$, shchurovskyite, $K_2CaCu_6(AsO_4)_4O_2$, and dmisokolovite, $K_3Cu_5Al(AsO_4)O_2$, are characterized by the presence of 'additional' oxygen atoms and thus may be described in terms of anion-centered tetrahedra (Krivovichev & Filatov, 2001; **Krivovichev *et al.*, 2013 [two Krivovichev et al. 2013 references, please indicate which]**). Within this approach, the crystal-chemical formula of the title compound can be written as (for Z = 2) $Rb_2Ca[O^{IV}{}_2Cu_6](PO_4)_4$, where square brackets denote a structural unit formed by anion-centered tetrahedra (Roman numerals indicate the coordination number of the 'additional' oxygen atoms). The O4 atom is tetrahedrally coordinated by four Cu^{2+} cations with the average ⟨O4–Cu⟩ distance of **1.912 (X) Å.** The (OCu_4) tetrahedra are linked *via* common Cu2···Cu3 edges forming a $[O_2Cu_6]^{8+}$ dimer [Fig. 6(*a*)]. The arrangement of isolated anion-centered dimers

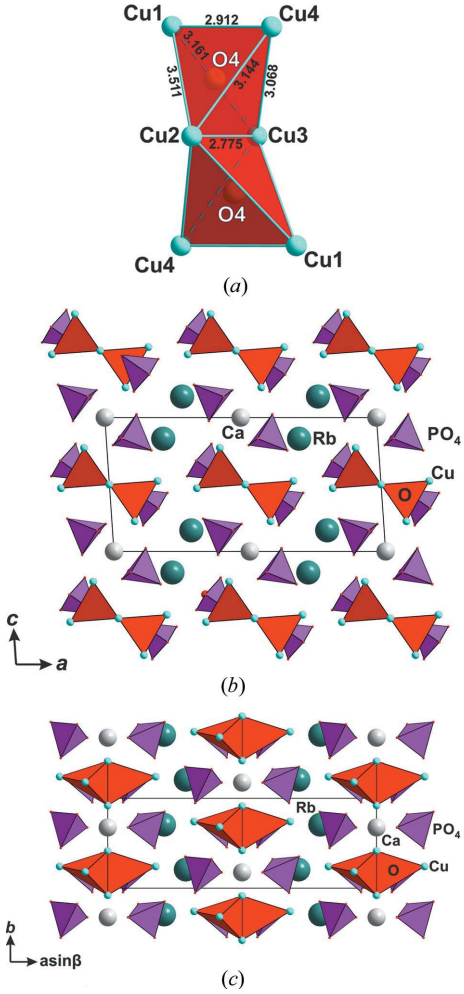

Figure 6
Anion-centered $[O_2Cu_6]$ dimer **Distances in Å. Why are s.u.'s missing on distances? These numbers are too small and should be given in caption.** (*a*) and general view of the crystal structure of $Rb_2CaCu_6(PO_4)_4O_2$ projected on (010) (*b*) and (001) (*c*).

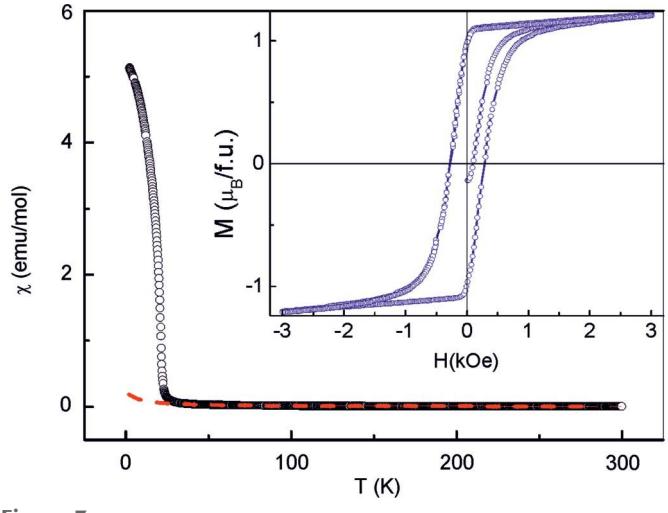

Figure 7
Temperature dependence of d.c. magnetic susceptibility $\chi = M/B$ **M/H?** in $Rb_2CaCu_6(PO_4)_4O_2$ taken at H = 80 kA m^{-1} (1000 Oe) in the field-cooled mode. The inset represents the hysteresis loop taken at T = 2 K.

and PO_4 tetrahedra as well as Rb^+ and Ca^{2+} cations is shown in Figs. 6(*b*) and 6(*c*).

3.2. Magnetic properties of $Rb_2CaCu_6(PO_4)_4O_2$: experiment

Magnetic properties of the collection of non-oriented tiny single crystals of $Rb_2CaCu_6(PO_4)_4O_2$ of total mass 3.73 mg were measured using the VSM option of the Physical Properties Measurements System PPMS (Quantum Design) 9 T. The temperature dependence of d.c. magnetic susceptibility $\chi = M/H$ taken in the field-cooled regime at $H = 80$ kA m^{-1} (1000 Oe) in the range 2–300 K is shown in Fig. 7. A sharp upturn in magnetization at $T_C = 25$ K signals transition into a long-range-ordered state with spontaneous magnetic moment. This is confirmed by the sharp hysteresis loop taken at $T = 2$ K, as shown in the inset to Fig. 7. The residual magnetization equals $M_R = 1.1$ μ_B per formula unit and the coercive force is 22.4 kA m^{-1}, which places $Rb_2CaCu_6(PO_4)_4O_2$ beyond the range of magnetically soft materials.

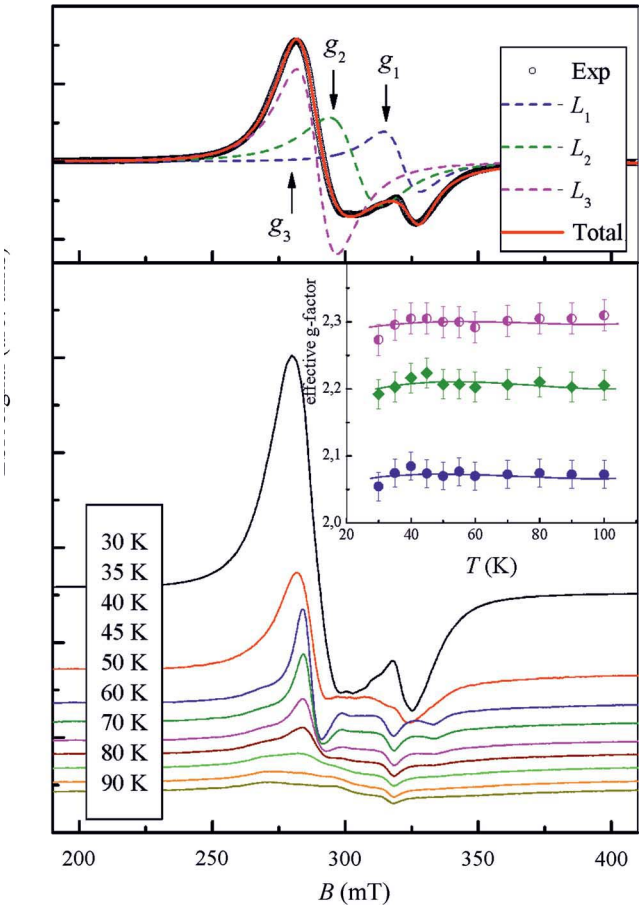

Figure 8
(Upper panel) Representative ESR spectrum of $Rb_2CaCu_6(PO_4)_4O_2$ with the fitting curves as described in the text. The dashed lines show the individual Lorentzian fit components and the solid line is the sum of all three. (Lower panel) The temperature evolution of ESR spectra of $Rb_2CaCu_6(PO_4)_4O_2$. Inset: the temperature dependence of principal values of the *g*-tensor.

Table 5
Calculated spin-independent (A) and spin-dependent (J) exchange parameters of the spin Hamiltonian $A - J\mathbf{S}_A\mathbf{S}_B$ for Cu^{2+}(A)···Cu^{2+}(B) exchange-coupled pairs in $Rb_2Ca\{Cu_6O_2(PO_4)_4\}$ (see Fig. 2 and Fig. 3).

	Exchange parameters (cm^{-1})		
Cu···Cu pair	A	J	J/A
Cu1···Cu1′	−1.23	+0.28	−0.23
Cu1···Cu2	−15.6	−3.9	0.25
Cu1···Cu3	−13.9	−21.8	1.57
Cu1···Cu4	−11.4	−6.0	0.53
Cu2···Cu3	−9.5	−36.0	3.79
Cu2···Cu4	−10.8	−19.1	1.77
Cu3···Cu4	−8.7	−12.7	1.46
Cu4···Cu4′ (interlayer)	−0.235	−0.055	0.23

At elevated temperatures, the $\chi(T)$ curve in $Rb_2CaCu_6(PO_4)_4O_2$ follows the Curie–Weiss law with inclusion of the temperature-independent term

$$\chi = \chi_0 + \frac{C}{T - \Theta}. \quad (4)$$

The fitting curve is shown by the dash in the main panel of **Fig. 1 [Fig. 7?]**. The parameters of the fitting in the range 120–300 K are $\chi_0 = -3.2 \times 10^{-4}$ emu mol^{-1} [**emu = electromagnetic unit?**], Curie constant $C = 1.74$ emuK mol^{-1} and Weiss temperature $\Theta = -$**7.2 K [delete minus sign?]**. The value of the temperature-independent term is somewhat less than the summation of individual diamagnetic Pascal's constants of constituent ions, equal to -3.8×10^{-4} emu mol^{-1} (Bain & Berry, 2008), which can be attributed to a paramagnetic van Vleck contribution of Cu^{2+} ions (Banks *et al.*, 2009). The value of the effective magnetic moment

$$\mu_{eff} = (8C)^{1/2}\mu_B \quad (5)$$

is equal to 3.73 μ_B which is to be compared with summation of the spin-only magnetic moments of six Cu^{2+} ions equal to 4.24 μ_B. The 10–20% reduction of the effective magnetic moment is a standard feature of copper-based low-dimensional magnetic systems (Vasiliev *et al.*, 2018). The low absolute value of the Weiss temperature, $\Theta =$ **−7.2 K**, as compared with the magnetic ordering temperature, $T_C = 25$ K, signifies fierce competition between ferromagnetic and antiferromagnetic exchange interactions in the title compound.

3.3. Electron spin resonance: experiment

An electron spin resonance (ESR) study of a powder sample of $Rb_2CaCu_6(PO_4)_4O_2$ was performed using an X-band ESR spectrometer CMS 8400 (ADANI) ($f \simeq 9.4$ GHz, $B \leq 0.7$ T) equipped with a low-temperature mount, operating in the range $T = 6$–300 K. The effective *g*-factors have been calculated with respect to a BDPA (*a*,*g*-bisdiphenyline-*b*-phenylallyl) reference sample with $g_{et} = 2.00359$. The main results are represented in Fig. 8. Typical ESR powder patterns of $Rb_2CaCu_6(PO_4)_4O_2$ in the paramagnetic phase are typical for Cu^{2+} ions with an anisotropic *g*-tensor. The amplitude of the signal increases monotonously upon cooling to 30 K, then

Table 6
Mineral and inorganic compounds with the shchurovskyite-type structure.

FD – framework density, number of framework cations per 1000 Å^3.

Mineral/compound	Space group	Z	Unit-cell parameters a (Å)	b (Å)	c (Å)	β (°)	V (Å^3)	FD
Shchurovskyite† $K_2Ca\{Cu_6O_2(AsO_4)_4\}$	$C2$	2	17.2856	5.6705	8.5734	92.953	839.24	23.8
Dmisokolovite† $K_3\{Cu_5AlO_2(AsO_4)_4\}$	$C2/c$	4	17.0848	5.7188	16.5332	91.716	1617.7	24.7
$Rb_2Ca\{Cu_6O_2(PO_4)_4\}$	$C2$	2	16.8913	5.6406	8.3591	93.919	794.57	25.17

† Pekov *et al.* (2015).

the signal degrades due to the onset of long-range magnetic order at T_C = 25 K.

In order to evaluate the main ESR parameters the experimental spectra were fitted by the sum of three components corresponding to the principal values of the g-tensor using three Lorentzian profiles. A representative example of the line-shape analysis is given in the upper panel of Fig. 8 with the resolved resonance modes denoted by dashed lines and their sum shown by the solid line. The presence of three different components obviously indicates the reduced symmetry of the crystal environment as compared with cubic symmetry and is typical for Cu^{2+} either in trigonally distorted octahedral, square-planar or square-pyramidal coordination (Krishna & Gupta, 1994). The principal g-values of the anisotropic g-tensor remain almost temperature independent over the whole temperature range investigated, with values g_1 = 2.07±0.01, g_2 = 2.20±0.01 and g_3 = 2.31±0.01 resulting in averaged g_{av} = 2.20±0.02, which is consistent with typical values for Cu^{2+} ions in other copper oxides (Zakharov *et al.*, 2014; Danilovich *et al.*, 2019). Remarkably, the obtained experimental g-values agree quite well with the theoretically calculated ones listed in Table 4. Note, it is impossible to resolve the signals from different Cu sites since the experimental absorption line is relatively broad and overlapping in nature. The slight deviation of the g-factors from their high-temperature values is indicative of the development of internal fields upon approach to the long-range-ordered phase.

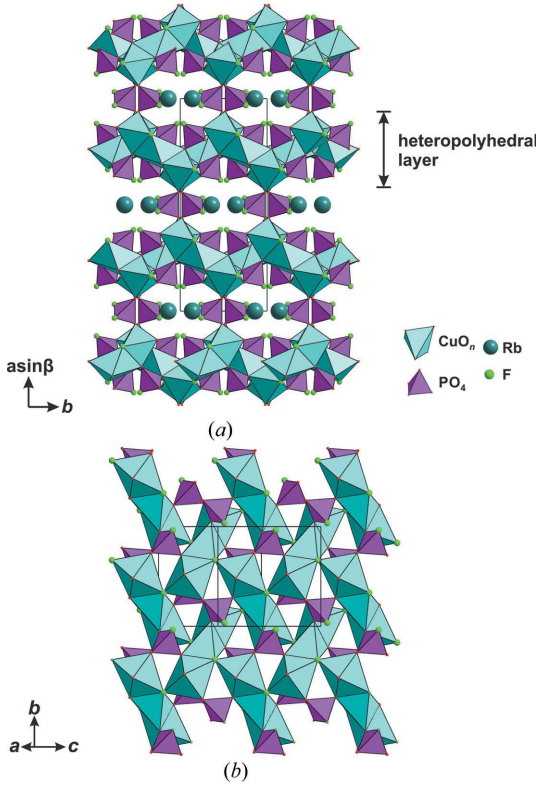

Figure 9
General view of the crystal structure of $RbCu_3(PO_2F_2)(PO_3F)_2F_2$ projected on (001) (*a*) and the heteropolyhedral copper phosphate layer (*b*).

3.4. Magnetic properties of $Rb_2CaCu_6(PO_4)_4O_2$: estimates of Cu–Cu exchange parameters

The presence of the 2D heteropolyhedral Cu-based layers in the crystal structure of $Rb_2CaCu_6(PO_4)_4O_2$ suggests low-dimensional magnetic properties of this compound (Takahashi, 1986). LF/AOM calculations indicate that Cu^{2+} ions in the copper sites Cu(1–4) have one unpaired electron occupying a magnetic 3*d* orbital of the x^2–y^2 type; the calculated components of the anisotropic g-tensor of the copper sites Cu(1–4) are listed in Table 5. These g-values are typical of Jahn–Teller Cu^{2+} ions with the basic square-planar CuO_4 coordination in the equatorial plane (with four short Cu—O bonds) and more distant apical oxygen atoms.

Spin coupling between two unpaired electrons on x^2–y^2 magnetic orbitals centered on two Cu^{2+} ions depends strongly on the character of the bridging groups and mutual spatial orientation of the two x^2–y^2 magnetic orbitals on the Cu^{2+}(A) and Cu^{2+}(B) ions (which is specified by orientation of the two CuO_4 square units). Coplanar orientation of neighboring CuO_4 squares favors dominant antiferromagnetic (AF) spin coupling, while non-coplanar orientation results in some ferromagnetic (F) superexchange pathways between half-

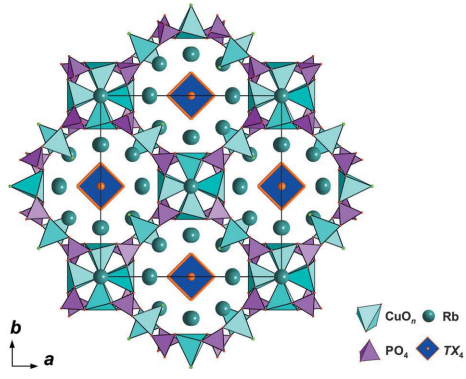

Figure 10
Crystal structures of a family of microporous copper diphosphates with general formula $A_9Cu_6(P_2O_7)_4Cl_3{\cdot}(TX_4)$.

Table 7
Crystallographic data and complexity parameters for rubidium copper phosphates.

Compound	Space group	Z	Unit-cell parameters: a (Å), α (°)	b (Å), β (°)	c (Å), γ (°)	V (Å^3)	FD	v (atoms)	I_G (bits per atoms)	$I_{G,total}$ (bits per unit cell)
Orthophosphates										
α-$RbCu(PO_4)$[a]	$Pc2_1n$	4	8.526	5.356	8.906	406.73	19.67	28	2.807	78.606
β-$RbCu(PO_4)$[b]	$P2_1$	4	8.603	9.659, 91.422	5.054	419.84	19.05	28	3.807	106.606
$Rb_2Cu(H_2PO_4)_4$[c]	$P\bar{1}$	1	6.970, 83.60	7.488, 71.78	7.923, 85.39	389.88		31	3.986	123.580
$Rb_2Cu(VO_2)_2(PO_4)_2$[d]	$P2_1/c$	2	4.929	11.471, 93.535	9.481	535.06	18.69	38	3.301	125.421
$Rb_2CaCu_6(PO_4)_4O_2$	$C2$	2	16.8913	5.6406, 93.919	8.3591	794.57	25.17	31	4.051	125.580
$RbCu_3(PO_2F_2)(PO_3F)_2F_2$[e,f]	$C2/c$	4	19.090	7.572, 103.683	7.819	1098.19	21.85	42	3.535	148.477
$Rb_2Cu_3(PO_3F)_4$[e, f]	$P2_1/c$	2	7.749	9.434, 95.186	9.219	671.2		50	3.684	184.193
$RbCuFe(PO_4)_2$[g]	$P2_1/n$	4	8.054	9.906, 115.47	9.140	658.34	24.30	52	3.700	192.423
$RbCuAl(PO_4)_2$[h]	$P2_1/c$	4	5.072	14.070, 100.41	9.352	656.44	24.37	52	3.700	192.423
γ-$RbCu(PO_4)$[b]	$Pnma$	12	8.932	16.118	8.567	1233.27	19.46	84	3.630	304.955
$Rb_2Cu_3(PO_2F_2)_2(PO_3F)$ (*sic*)[e]†	$P2_1/n$	n.d.	5.383	14.191, 91.83	15.888	1213.13				
Diphosphates										
β-$Rb_2Cu(P_2O_7)$[i]	Cc	4	7.002	12.751, 110.93	9.773	815.0	14.72	24	3.585	86.039
$Rb_{1.5}(NH_4)_{0.5}Cu(P_2O_7)$[j]	$Pmcn$	2	5.183	10.096	15.146	792.58		48	3.252	156.078
$Rb_2Cu_3(P_2O_7)_2$[k]	$P2_1/c$	2	7.712	10.525, 103.862	7.803	614.91	16.26	46	3.567	164.084
$Rb_9Cu_6(P_2O_7)_4Cl_3\cdot(CuCl_4)$[l]	$I4/mcm$	4	17.843	17.843	13.493	4295.96	13.04	118	3.510	414.152
$Rb_9Cu_6(P_2O_7)_4Cl_3\cdot(Au_{1.54}Cl_{5.12})$[l]	$I4/mcm$	4	17.874	17.874	13.480	4306.65	13.00	124	3.664	454.320
$Rb_9Cu_6(P_2O_7)_4Cl_3\cdot(Au_{0.535}Cl_{3.27})$[l]	$I4/mcm$	4	17.770	17.770	13.455	4248.7	13.18	128	3.656	480.000
$(Rb,K)_2Cu_3(P_2O_7)_2$[m]	$P2_12_12_1$	8	9.941	13.475	18.635	2496.4	22.43	184	5.524	1016.335

[a] Henry *et al.* (2000); [b] Henry *et al.* (2010); [c] Chaouche *et al.* (2010); [d] Yakubovich *et al.* (2008); [e] Armstrong *et al.* (2011); [f] Williams *et al.* (2012); [g] Badri *et al.* (2013); [h] Yakubovich *et al.* (2016); [i] Shvanskaya *et al.* (2012); [j] Chernyatieva *et al.* (2019); [k] Shvanskaya *et al.* (2013); [l] Williams *et al.* (2013); [m] Krivovichev & Chernyat'eva (2016). † Because of the absence of crystal structure data, we are not able to calculate FD value and complexity parameters. Moreover, the reported chemical formula is not charge balanced.

filled x^2–y^2 orbitals and other doubly occupied d orbitals. Given that in most of the Cu···Cu pairs in the crystal structure of $Rb_2CaCu_6(PO_4)_4O_2$ the CuO_4 units are non-coplanar, some competition between F and AF contributions might be expected, which would tend to reduce the overall magnitude of the exchange parameter J. More quantitatively, the AF versus F competition is measured by the ratio between the spin-independent (A) and spin-dependent (J) exchange parameters in the full spin Hamiltonian $H = A - J\mathbf{S}_A\mathbf{S}_B$ resulting from the superexchange mechanism.

For the spin $S = 1/2$ of Cu^{2+} ions, the AF contributions are described by the $J(1/4 - \mathbf{S}_A\mathbf{S}_B)$ spin Hamiltonian with the $J/A = 4$ ratio; for the F contribution this ratio is negative. Thus, generally we have $J/A < 4$. Therefore, the J/A ratio reflects the degree of the AF/F competition in the Cu···Cu pairs: the smaller the J/A, the stronger the F contributions, which dominate at $J/A < 0$. With this in mind, we calculated the A and J exchange parameters for all actual exchange-coupled pairs Cu···Cu in $Rb_2CaCu_6(PO_4)_4O_2$ (Table 6).

These data show that, except for the Cu2–Cu3 pairs (J/A = 3.76), the ratio J/A is considerably less than 4, thereby indicating strong F/AF competition in the exchange-coupled pairs. This is consistent with the non-coplanar orientation of the CuO_4 square units with short Cu—O bonds in most of the Cu···Cu pairs. It is also noteworthy that the small value of the spin-independent exchange parameter A necessarily implies a small spin-dependent (conventional) exchange parameter J owing to the relation $J/A \leq 4$; in other words, a small A value indicates poor efficiency of the bridging groups as mediators of the spin coupling between two magnetic centers Cu^{2+}(A) and Cu^{2+}(B) (which manifests in small electron transfer parameters t_{ij}). This situation occurs for the Cu1···Cu1′ pairs within the copper layer and for the Cu4···Cu4′ pairs connecting two neighboring copper layers, in which a small parameter A combines with a low J/A ratio, ultimately resulting in very weak spin coupling (J = +0.28 and J = −0.05 cm^{-1}, respectively, Table 6). It is important to note that these pairs play a key role in the overall magnetic behavior of $Rb_2CaCu_6(PO_4)_4O_2$ as they determine magnetic connectivity within the copper layers (the Cu1···Cu1′ pair, weakly ferromagnetic spin coupling with J = +0.28 cm^{-1}) and magnetic coupling between the copper layers (the Cu4···Cu4′ pair, weak AF spin coupling, J = −0.05 cm^{-1}). By contrast, the Cu2···Cu3 pairs in the rods composed of edge-sharing CuO_4 squares exhibit a moderately strong AF spin coupling (J = −36.0 cm^{-1}) with a large J/A = 3.79 ratio (which is close to the limiting value of 4), indicating dominant AF contributions. This fact is consistent with the coplanar orientation of edge-sharing CuO_4 squares and with the presence of two bridging O atoms with short Cu—O bonds, which are good mediators of spin coupling between Cu^{2+} ions in the Cu2 and Cu3 sites. Exchange interactions between these copper sites and 'decorating' Cu1 and Cu4 sites are all antiferromagnetic with a rather low J/A ratio (< 2); again, this indicates a pronounced competition between AF and F superexchange pathways in the pairs caused by the non-coplanar orientation of the CuO_4 squares.

4. Discussion

$Rb_2CaCu_6(PO_4)_4O_2$ belongs to the group of rubidium copper phosphates (Table 6) and is related to fluorophosphates

$RbCu_3(PO_2F_2)(PO_3F)_2F_2$ and $Rb_2Cu_3(PO_2F_2)_2(PO_3F)$ (*sic*) (Armstrong *et al.*, 2011), which both possess structures based upon heteropolyhedral frameworks. The first compound consists of heteropolyhedral mixed copper phosphate layers linked *via* isolated $PØ_4$ tetrahedra (Ø = O, F) [Fig. 9(*a*)]. Layers are formed by $[Cu_3O_8F_4]$ trimers of face-sharing $CuØ_6$ octahedra and $PØ_4$ tetrahedra [Fig. 9(*b*)]. Armstrong *et al.* (2011) reported that the crystal structure of $Rb_2Cu_3(PO_2F_2)_2(PO_3F)$ is based upon infinite chains of CuO_4F square-based pyramids and CuO_5F octahedra, which are linked by PO_3F tetrahedra. Unfortunately, there is no further information concerning the crystal structure of this compound. The chemical formula $Rb_2Cu_3(PO_2F_2)_2(PO_3F)$ is notably non-electroneutral, assuming a divalent state of Cu.

Except for $Rb_2Cu(H_2PO_4)$ (Chaouche *et al.*, 2010) and $Rb_2Cu_3(PO_3F)_4$ (Armstrong *et al.*, 2011), all rubidium copper phosphates have microporous structures with low framework densities from 13.00 to 25.17 Cu+**M [Me = metal?]**+P atoms per 1 nm^3 (Table 6). Among these, the family of diphosphates with the general formula $A_9Cu_6(P_2O_7)_4Cl_3{\cdot}(TX_4)$ (where A = K^+, Rb^+, Cs^+; T = P^{5+}, Cu^{2+}, Pt^{2+}, Pd^{2+}, Au^{3+}; X = O^{2-}, OH^-, Cl^-, Br^-) (Williams *et al.*, 2013) (Fig. 10) is characterized by very low framework densities of ∼13.1 (1). Their $\{Cu_6(P_2O_7)_4Cl_3\}^{7-}$ open frameworks contain large channels filled by alkaline **earth?** cations and tetrahedral or planar (TX_4) anions. [**Table 7 not yet cited, please include a citation**]

5. Conclusion

Single crystals of $Rb_2CaCu_6(PO_4)_4O_2$ were synthesized by a hydrothermal method. The crystal structure of $Rb_2CaCu_6(PO_4)_4O_2$ is similar to those of shchurovskyite and dmisokolovite and is based on a heteropolyhedral open framework formed by polar copper layers linked *via* isolated PO_4 tetrahedra. The results of our microscopic calculations in terms of a many-electron superexchange model are indicative of possible low-dimensional magnetic behavior of the title material, since they confirm weak magnetic coupling between the Cu-based layers mediated by the Cu4···Cu4′ pairs (J = $-0.05\ cm^{-1}$). However, the actual character of the low-dimensional magnetism (1D or 2D) is rather uncertain, owing to the presence of weak exchange interactions within the layers (*i.e.* weakly ferromagnetic Cu1···**Cu1′** pairs, J = $+0.28\ cm^{-1}$), which may destroy magnetic connectivity within the copper 2D network and thus tends to further reduce the efficient dimensionality of the magnetic system. The calculated values of the principal components of the g-tensor nicely correspond to averaged values of g-factors defined experimentally. The low-dimensional magnetic behavior of the title compound is masked by the fierce competition between multiple ferromagnetic and antiferromagnetic exchange interactions. At T_C = 25 K, $Rb_2CaCu_6(PO_4)_4O_2$ reaches a magnetically ordered state with large residual magnetization M_R. Taking into account the even number of magnetic ions per formula unit one may presume the non-collinear magnetic structure **exists** at $T < T_C$, which is to be verified in neutron scattering measurements.

Funding information

SMA and DVD thank the Foundation of the President of the Russian Federation (grant No. MK-3502.2018.5). VSM is grateful for support by the Federal Agency of Scientific Organizations (agreement No 007-G3/3363/26) for the magnetic calculations. ASV and **OVG [OAG?]** thank the Russian Foundation for Basic Research (grant No. 17-13-00886-a). SVK is grateful to the Council of Grants of the President of the Russian Federation for financial support (grant No. 3079.2018.5). PCB's participation was supported by the Chemical Sciences, Geosciences and Biosciences Division, Office of Basic Energy Sciences, Office of Science, US Department of Energy, Grant No. DE-FG02-07ER15880. Support from the Russian Science Foundation (grant 19-42-02010) is acknowledged. This work has also been supported by the Ministry of Education and Science of the Russian Federation through NUST 'MISiS' grant K2-2017-084 and by the Act 211 of the Government of Russia, contracts 02.A03.21.0004 and 02.A03.21.0011.

References

Aksenov, S. M., Mironov, V. S., Borovikova, E. Yu., Yamnova, N. A., Gurbanova, O. A., Volkov, A. S., Dimitrova, O. V. & Deyneko, D. V. (2017). *Solid State Sci.* **63**, 16–22.

Armstrong, J. A., Williams, E. R. & Weller, M. T. (2011). *J. Am. Chem. Soc.* **133**, 8252–8263.

Badri, A., Hidouri, M. & Ben Amara, M. (2013). *Acta Cryst.* E**69**, i52.

Bain, G. A. & Berry, J. F. (2008). *J. Chem. Educ.* **85**, 532.

Banks, M. G., Kremer, R. K., Hoch, C., Simon, A., Ouladdiaf, B., Broto, J. M., Rakoto, H., Lee, C. & Whangbo, M. H. (2009). *Phys. Rev. B*, **80**, 024404.

Blatov, V. A., Shevchenko, A. P. & Proserpio, D. M. (2014). *Cryst. Growth Des.* **14**, 3576–3586.

Brandenburg, K. & Putz, H. (2005). *DIAMOND*, Version 3. Crystal Impact GbR, Bonn, Germany.

Brown, I. D. & Altermatt, D. (1985). *Acta Cryst.* B**41**, 244–247.

Burns, P. C. & Hawthorne, F. C. (1995*a*). *Can. Mineral.* **33**, 889**–905**.

Burns, P. C. & Hawthorne, F. C. (1995*b*). *Can. Mineral.* **33**, 1177**–1188**.

Chaouche, S., Ouarsal, R., Bali, B. E., Lachkar, M., Bolte, M. & Dusek, M. (2010). *J. Chem. Crystallogr.* **40**, 526–530.

Cheetham, A. K., Férey, G. & Loiseau, T. (1999). *Angew. Chem.* **111**, 3466–3492.

Chernyatieva, A. P., Aksenov, S. M., Krivovichev, S. V., Yamnova, N. A. & Burns, P. C. (2019). *Crystallogr. Rep.* **64**, 239–246.

Danilovich, I. L., Merkulova, A. V., Morozov, I. V., Ovchenkov, E. A., Spiridonov, F. M., Zvereva, E. A., Volkova, O. S., Mazurenko, V. V., Pchelkina, Z. V., Tsirlin, A. A., Balz, C., Holenstein, S., Luetkens, H., Shakin, A. A. & Vasiliev, A. N. (2019). *J. Alloys Compd.* **776**, 16–21.

Grew, E. S., Krivovichev, S. V., Hazen, R. M. & Hystad, G. (2016). *Can. Mineral.* **54**, 125–143.

Hazen, R. M., Grew, E. S., Origlieri, M. J. & Downs, R. T. (2017). *Am. Mineral.* **102**, 595–611.

Henry, P. F., Hughes, R. W., Ward, S. C. & Weller, M. T. (2000). *Chem. Commun.* pp. 1959–1960.

Henry, P. F., Kimber, S. A. J. & Argyriou, D. N. (2010). *Acta Cryst.* B**66**, 412–421.

Prince, E. (2006). Editor. *International Tables for Crystallography*, Vol. C, *Mathematical, Physical and Chemical Tables*. International Union of Crystallography.

Krishna, R. M. & Gupta, S. K. (1994). *Bull. Magn. Reson.* **16**, 239–**291**.
Krivovichev, S. V. (2012*a*). *Z. Kristallogr.* **227**, 575–**579**.
Krivovichev, S. (2012*b*). *Acta Cryst.* A**68**, 393–398.
Krivovichev, S. V. (2013*a*). *Mineral. Mag.* **77**, 275–326.
Krivovichev, S. V. (2013*b*). *Microporous Mesoporous Mater.* **171**, 223–229.
Krivovichev, S. V. & Chernyat'eva, A. P. (2016). *Glass Phys. Chem.* **42**, 327–336.
Krivovichev, S. V. & Filatov, S. K. (2001). *Crystal Chemistry of Minerals and Inorganic Compounds with Complexes of Anion-Centered Tetrahedra.* St Petersburg: St Petersburg University Press.
Krivovichev, S. V., Filatov, S. K. & Vergasova, L. P. (2013). *Mineral. Petrol.* **107**, 235–242.
Krivovichev, S. V., Mentré, O., Siidra, O., Colmont, M. & Filatov, S. K. (2013). *Chem. Rev.* **113**, 6459–6535.
Lee, S. J. (1989). *J. Am. Chem. Soc.* **111**, 7754–7761.
Leonyuk, L., Babonas, G.-J., Pushcharovskii, D. Yu. & Maltsev, V. (1998). *Crystallogr. Rep.* **43**, 256–**270**.
Leonyuk, L., Maltsev, V., Babonas, G.-J., Szymczak, R., Szymczak, H. & Baran, M. (2001). *Acta Cryst.* A**57**, 34–39.
Mannasova *et al.* (2016). **Please provide full reference details including names and initials of all authors.**
Maspoch, D., Ruiz-Molina, D. & Veciana, J. (2007). *Chem. Soc. Rev.* **36**, 770–818.
McCusker, L., Liebau, F. & Engelhardt, G. (2003). *Microporous Mesoporous Mater.* **58**, 3–13.
Mironov, V. S., Chibotaru, L. F. & Ceulemans, A. (2003). *Phys. Rev. B*, **67**, 014424.
Nikiforova, M. E., Kiskin, M. A., Bogomyakov, A. S., Aleksandrov, G. G., Sidorov, A. A., Mironov, V. S. & Eremenko, I. L. (2011). *Inorg. Chem. Commun.* **14**, 362–365.
Oxford Diffraction (2009). *CrysAlis PRO*. Oxford Diffraction Ltd, Abingdon, Oxfordshire, UK.
Palatinus, L. & Chapuis, G. (2007). *J. Appl. Cryst.* **40**, 786–790.
Pekov, I. V., Zubkova, N. V., Belakovskiy, D. I., Yapaskurt, V. O., Vigasina, M. F., Sidorov, E. G. & Pushcharovsky, D. Yu. (2015). *Mineral. Mag.* **79**, 1737–1753.
Pekov, I. V., Zubkova, N. V. & Pushcharovsky, D. Y. (2018). *Acta Cryst.* B**74**, 502–518.
Petříček, V., Dušek, M. & Palatinus, L. (2006). *Jana2006*, *structure determination software program*. Institute of Physics, Praha, Czech Republic.
Schaffer, C. E. (1968). *Struct. Bond.* **5**, 68–**95.**
Shvanskaya, L., Yakubovich, O., Ivanova, A., Baidya, S., Saha-Dasgupta, T., Zvereva, E., Golovanov, A., Volkova, O. & Vasiliev, A. (2013). *New J. Chem.* **37**, 2743–**2750**.
Shvanskaya, L. V., Yakubovich, O. V. & Urusov, V. S. (2012). *Dokl. Phys. Chem.* **442**, 19–26.
Siidra, O. I., Zenko, D. S. & Krivovichev, S. V. (2014). *Am. Mineral.* **99**, 817–823.
Takahashi, M. (1986). *Prog. Theor. Phys. Suppl.* **87**, 233–246.
Vasiliev, A., Volkova, O., Zvereva, E. & Markina, M. (2018). *NPJ Quantum Mater.* **3**, 18.
Volkova, L. M. & Marinin, D. V. (2017). *J. Supercond. Nov. Magn.* **30**, 959–971.
Volkova, L. M. & Marinin, D. V. (2018*a*). *Phys. Chem. Miner.* **45**, 655–668.
Volkova, L. M. & Marinin, D. V. (2018*b*). *J. Phys. Condens. Matter*, **30**, 425801.
Whittingham, M. S. (2014). *Chem. Rev.* **114**, 11414–11443.
Williams, E. R., Leithall, R. M., Raja, R. & Weller, M. T. (2013). *Chem. Commun.* **49**, 249–251.
Williams, E. R., Morris, S. A. & Weller, M. T. (2012). *Dalton Trans.* **41**, 10854.
Yakubovich, O. V., Kiriukhina, G. V., Dimitrova, O. V., Zvereva, E. A., Shvanskaya, L. V., Volkova, O. S. & Vasiliev, A. N. (2016). *Dalton Trans.* **45**, 2598–2604.
Yakubovich, O. V., Steele, I. M. & Dimitrova, O. V. (2008). *Acta Cryst.* C**64**, i62–i65.
Yamnova, N. A., Aksenov, S. M., Mironov, V. S., Volkov, A. S., Borovikova, E. Yu., Gurbanova, O. A., Dimitrova, O. V. & Deyneko, D. V. (2017). *Crystallogr. Rep.* **62**, 382–390.
Zakharov, K. V., Zvereva, E. A., Berdonosov, P. S., Kuznetsova, E. S., Dolgikh, V. A., Clark, L., Black, C., Lightfoot, P., Kockelmann, W., Pchelkina, Z. V., Streltsov, S. V., Volkova, O. S. & Vasiliev, A. N. (2014). *Phys. Rev. B*, **90**, 214417.
Zorina, E. N., Zauzolkova, N. V., Sidorov, A. A., Aleksandrov, G. G., Lermontov, A. S., Kiskin, M. A., Bogomyakov, A. S., Mironov, V. S., Novotortsev, V. M. & Eremenko, I. L. (2013). *Inorg. Chim. Acta*, **396**, 108–118.